A new look into 4-(2,3-dihydro-1,3-dimethyl-1H-benzimidazol-2-yl)-N,N-dimethylbenzenamine (DMBI-H) n-type dopant: not so stable after all, but it does not necessarily matter.

Francesca Pallini,[a] Sara Mattiello,[a] Marco Cassinelli,[b] Pietro Rossi,[b,c] Sara Mecca,[a] Mauro Sassi,[a] Guglielmo Lanzani,[b,c] Mario Caironi[b]* and Luca Beverina[a]*

4-(2,3-dihydro-1,3-dimethyl-1H-benzimidazol-2-yl)-N,N-dimethylbenzenamine (DMBI-H) is a very successful dopant for n-type organic semiconductors. It is efficient over a large range of polymers and small molecule derivatives, commercially available, soluble in established processing solvents and generally considered to be air stable. Yet, on a closer look not all that glisters is gold. We show that DMBI-H does indeed decompose in the processing solvent, but the process does not negatively impact performances. Its main decomposition product acts as a nucleating agent for DMBI-H with the overall effect of boosting conductivity of the final doped P(NDI2OD-T2) films. Such results, confirmed by control experiments performed with a different nucleating agent, shine a light on the crucial role played by solid-state microstructure in DMBI-H doped semiconductors and hints a viable way to its optimization.

The development of molecular doping is having a major impact in boosting the performances of nearly all plastic (opto)electronic devices.[1] The capability to tune the conductivity of both *p* and *n* type doped organic semiconductors over orders of magnitude, while at the same time improving energy level alignments between different organic materials and metallic contacts, proved to be game changing for vacuum processed OLEDs, OFETs, OPV devices[2–5] and in any case resourceful for the more challenging solution processed Organic Thermoelectric Generators (OTEGs).[6–10] Key to the success of the approach was the development of *p* and *n* dopants having a very general behaviour over a vast range of already developed, high mobility polymeric and small molecule materials.[3,11–13] p-type doping of hole transporting semiconductors is

[a] Department of Materials Science, Università di Milano-Bicocca, via Cozzi 55, 20125 Milan, Italy
[b] Center for Nano Science and Technology@PoliMi, Istituto Italiano di Tecnologia, via Giovanni Pascoli 70, 20133 Milan, Italy
[c] Physics Department, Politecnico di Milano, p.zza Leonardo da Vinci 32, 20133, Milan, Italy
Electronic Supplementary Information (ESI) available: synthetic procedures; additional data on DMBI-H degradation; additional DSC characterizations; details on electrical characterization; NMR of all derivatives. See DOI: 10.1039/x0xx00000x

energetically simpler due to the relatively high lying Highest Occupied Molecular Orbital (HOMO) levels of materials like polythiophenes. Fluorinated tetracyanoquinodimethane derivatives like F4TCNQ can be handled in the air and provide very efficient *p*-type doping in solution and in the solid state.[14,15] The *n*-type doped organic semiconductors are more challenging. Suitable dopants should feature HOMO levels higher than -3.8 eV, the energy more or less corresponding to the LUMO level of high electron mobility semiconductors like PCBM or P(NDI2OD-T2).[16–19] This clearly poses serious problems of air stability, not just for the doped polymer but for the dopant itself. A valuable approach to overcome this problem is the development of kinetically air-stable dopant precursors which, after incorporation into the host material, can be thermally or photochemically converted in more reductive species through bond formation/cleavage. DMBI-H is by far the most widely studied "precursor" dopant, particularly in the emerging field of OTGs.[19–22] Per se, DMBI-H is a fairly electron rich molecule (HOMO energy level at -4.4 eV), yet still energetically uncapable of doping neither $PC_{60}BM$ (LUMO level at -3.9 eV) nor P(NDI2OD-T2) (LUMO at -3.8 eV).[23]

The details of the doping mechanism upon which DMBI-H can end up donating one electron to an organic semiconductor are very much dependent upon the specific counterpart. In a series of very detailed papers, Marder and Bao convincingly demonstrated that the doping process in the case of fullerene derivatives is triggered by a hydride donation from DMBI-H, with formation of $DMBI^+$ cation (Scheme 1, path A). In other cases, the hydride donation is competitive with the homolytic cleavage of the C-H bond and the formation of a highly electron rich carbon centered radical, having a SOMO typically placed around – 2.40 eV and thus fully capable of n-type doping essentially all organic semiconductors (Scheme 1, path B). Yi very recently disclosed that the energetics for the heterolytic (hydride donation) and homolytic (hydrogen donation) C-H bond cleavage for the isolated molecule are essentially the same. Conversely, either one of the two competing processes can become dominant when assisted by the target *n*-dopable semiconductor. The specific chemical nature of the semiconductor and the details of the interaction geometry determine the preferential pathway.[20,23–25] Whatever the details of the doping mechanism(s), the two main attractive features generally attributed to DMBI-H are generality and air stability. The first one is demonstrated but the second is questionable.[26]

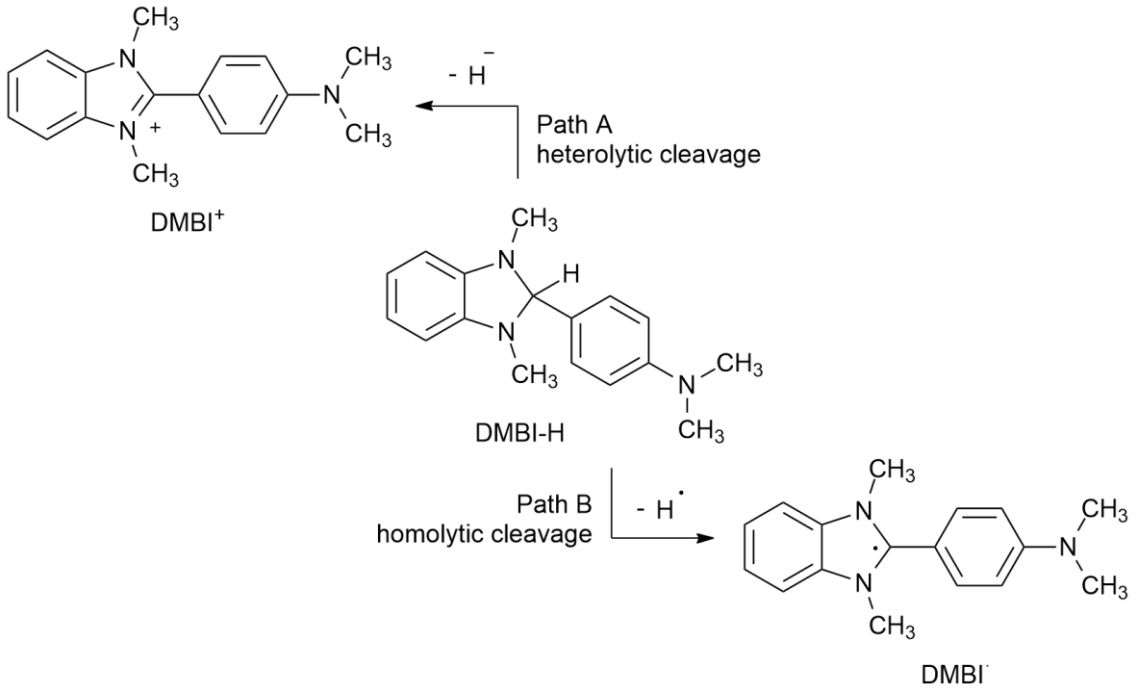

Scheme 1. Possible cleavage mechanisms of DMBI-H, with formation of different reducing species: hydride (heterolytic cleavage, path A) and DMBI$^{\bullet}$ radical (homolytic cleavage, path B)

In this paper we show the evolution over time of the NMR spectra of carefully purified samples of DMBI-H as solution in the processing solvent. We characterize and isolate the most relevant byproduct thus formed and we evaluate the impact of its presence in DMBI-H/P(NDI2OD-T2) blends. Our findings show that the nature of such product differs from the one expected on the basis of the accepted doping mechanism.[23] Even more surprisingly, data show that its presence sizeably helps performances, particularly at low doping levels. The most likely explanation for the unexpected behaviour is a seeded crystallization of DMBI-H in very small crystallites within P(NDI2OD-T2). To substantiate the hypothesis, we tested a series of P(NDI2OD-T2) blends with an electrochemically inert nucleating agent. We show that the presence of the nucleating agent enables a 2-to-5-fold increase in the blend electrical conductivity with respect to control experiments having the same dopant concentration.

Synthesis and purification of DMBI-H.

Scheme 2 summarizes all literature approaches at the preparation of DMBI-H. The most popular route, frequently employed for the preparation of DMBI-like compounds having a different

substitution pattern at the amino-residue, starts from *N*,*N'*-dimethyl-1,2-phenylenediamine **3**.[21,23] The latter is commercially available but rather expensive and prone to oxidative degradation. 1,2-phenylenediamine is converted to the corresponding sulphonamide **1** by reaction with tosyl chloride in dichloromethane (DCM). Deprotonation of **1** in DMF, followed by alkylation with methyl iodide, gives product **2**. Hydrolysis in concentrated sulphuric acid at high temperature, followed by neutralization, gives **3** after chromatographic purification. The final step in the preparation of DMBI-H is an acid catalysed condensation between **3** and 4-(dimethylamino)benzaldehyde. The process is in some cases described to be assisted by ultrasound. DMBI-H precipitates, is collected by filtration and in some cases further purified by crystallization (Scheme 2, path A). The overall yield is just above 18%.

Alternatively, it is possible to react directly 1,2-phenylenediamine with 4-(dimethylamino)benzaldehyde to give the 2-arylbenzimidazole **4** in moderate yield. The same gives iodide **5** after double alkylation with methyl iodide under alkaline conditions, later converted in the corresponding triflate **6** by metathesis with the corresponding silver salt.[27]

The anion exchange is necessary to avoid reduction of iodide during the following step, requiring a treatment with $NaBH_4$ to give the final product in an overall yield of almost 23%. The main advantage of pathway B is the possibility to change the substitution pattern on the benzimidazole residue by using alkylating agents other than methyl iodide.

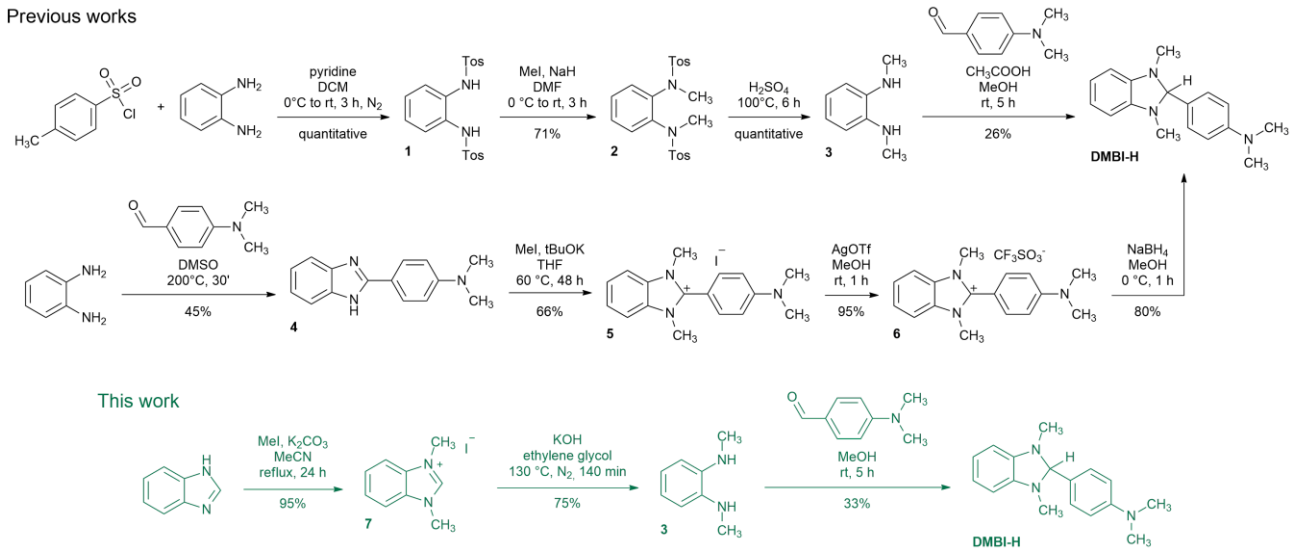

Scheme 2. Literature routes toward the synthesis of DMBI-H (in black), and improved synthesis of amine **3** and DMBI-H proposed in this work (in green).

If it were not for the expensiveness of **3**, path A would be preferable. We thus developed an alternative synthesis of **3**, more respectful of atom economy, and improved the subsequent condensation. As it is shown in Scheme 2, inexpensive benzimidazole can be alkylated in essentially quantitative yield with methyl iodide/K_2CO_3 to give iodide **7**. High temperature alkaline hydrolysis of **7** affords **3** in 75% yield after vacuum distillation. To the best of our knowledge, the preparative application of such protocol is original.[28] The usual acid catalysed condensation gives analytically pure DMBI-H, after a short silica gel filtration.

During purification, we realized how delicate DMBI-H is in solution, especially under standard laboratory atmosphere. This finding prompted us to challenge the numerous reports describing the pretended ambient stability of DMBI-H, particularly when dissolved in chlorinated solvents.

(In)stability of DMBI-H.

Pure DMBI-H is a pale yellow crystalline solid that darkens upon storage under air. Commercial samples might be already significantly darkened at first opening. In our experience, pure samples kept under argon and in the dark can be stored for months without hints of degradation, but samples left under laboratory atmosphere darkens in a few days (see ESI). We will extensively comment on the impact of such a degradation in the next section.

Both DMBI-H and P(NDI2OD-T2) are soluble in a wide range of solvents. It is however common practice to perform doping experiments in either chloro- or o-dichlorobenzene for the sake of the overall film quality. Doping experiments are not consistently performed in the literature, with relevant changes in the experimental protocol regarding solvent purity, control of the environment, time and temperature of thermal treatments, sequence of the operations. We dissolved DMBI-H at 10 mg/mL in d_5-chlorobenzene saturated with argon and we prepared two distinct NMR tubes: one sealed under argon atmosphere (Sample Ar) and one under standard laboratory atmosphere (Sample O_2). We then monitored the corresponding ^{1}H NMR spectra as the function of the elapsed time at room temperature.

Figure 1A shows the evolution of the NMR spectra of sample O_2 within the first 9 days. The formation of a degradation product is evident after a few hours, with complete conversion requiring 9 days. We isolated and extensively characterized the main decomposition product, to a somewhat unexpected result. The ^{1}H NMR characterization shows a mixture of two

compounds in roughly 1:9 molar ratio: the cation $DMBI^+$ (5 mol%, Scheme 1) and the amide DMBI-Ox (95 mol%, Figure 1C).

The details of the mechanism of formation of DMBI-Ox, a compound that can be considered in equilibrium with the more commonly reported cation $DMBI^+$, are not known as the presence of an oxygen atom could be traced back to both O_2 and water dissolved in the NMR solvent. We however proved that the process is started by reaction with molecular oxygen as the identical NMR sample, which we prepared and stored under Ar (Sample Ar) for the whole time, displayed a dramatically slower decomposition kinetics. As it is shown in Figure 1B, after 2 days the O_2 sample is already 50% decomposed while the Ar one is still barely showing appreciable evolution. Later on, even the Ar sample decomposed, likewise because of reaction with O_2 traces in the glove box (O_2 and H_2O concentration in the 1-5 and 0.1-0.5 ppm level during the experiment).

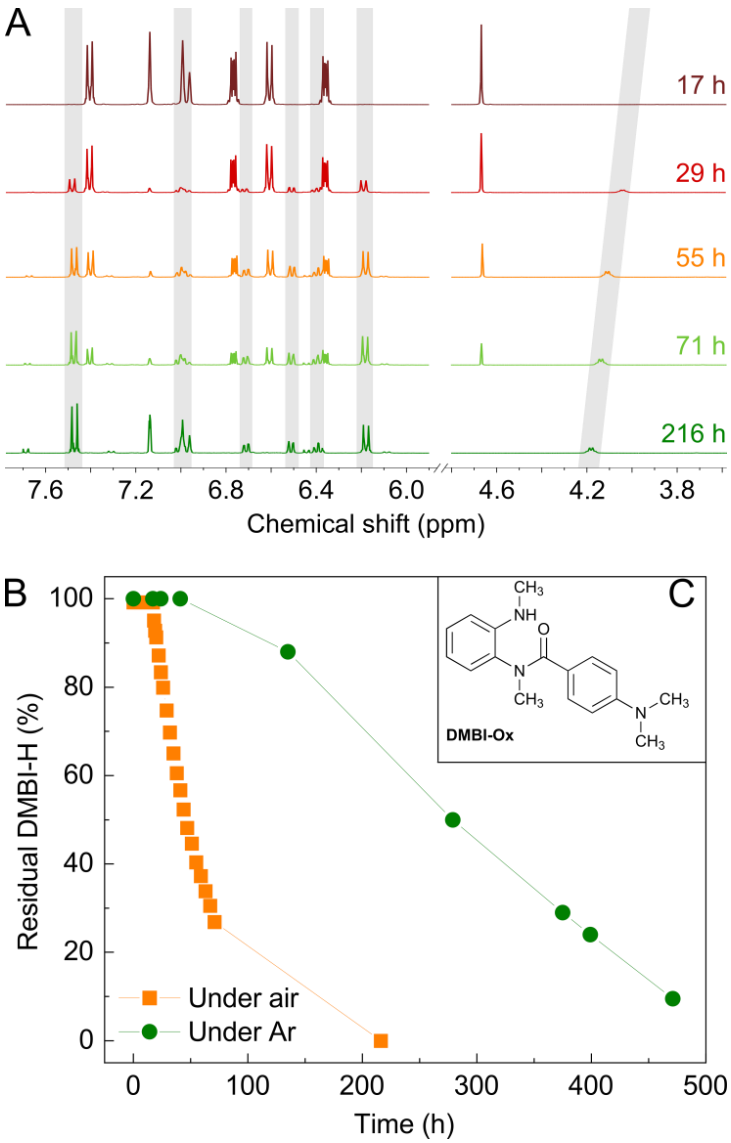

Figure 1. A) Time evolution of the ^{1}H NMR spectra of a solution of DMBI-H in d_5-chlorobenzene under laboratory atmosphere. Peaks at 6.96, 6.99 and 7.14 ppm are solvent residual signals. The grey rectangles highlight the peaks of the forming species DMBI-Ox. B) Degradation over time of DMBI-H in deuterated chlorobenzene estimated by ^{1}H NMR for a sample prepared under laboratory atmosphere (orange squares) and under Ar (green circles). The inset C shows the structure of the principal identified degradation product, DMBI-Ox.

As we have mentioned, some authors go to a great length to ensure purity and correct handling of the samples, while others do not pay equal attention because of the supposed stability of DMBI-H.[21,29–32] And yet, performances are surprisingly consistent when the doping is performed on the same polymers. Puzzled, we decided to run a series of comparative tests on different samples of DMBI-H coming from the same batch but aged for a different time under the same

conditions and we compared the results with samples intentionally contaminated with known quantities of DMBI-Ox.

Electrical and thermal characterization of DMBI-H/P(NDI2OD-T2) blends as a function of the DMBI-Ox concentration.

We prepared 5 blends of DMBI-H/P(NDI2OD-T2) at 1, 3, 5, 10, 30 wt% composition, all of them dissolved at identical polymer concentration in chlorobenzene under inert atmosphere in the glove box. Samples were stored under conditions identical to those of the NMR-Ar previously discussed and at precise interval times thin films were made by spin coating and thermally annealed under the same conditions (see experimental). We thus compared electrical conductivity (σ) values as a function of time and dopant concentration (Figure 2). The dopant concentration dependency was very much in line with our previous experience with DMBI-H/P(NDI2OD-T2) blends.[21] On the contrary, the time dependence was unexpected. For the first 250 h of aging, we did not monitor any decrease in the conductivity, and only after 400 h some of the samples did show a decrease, in any case negligible, except for the 1 wt% sample.

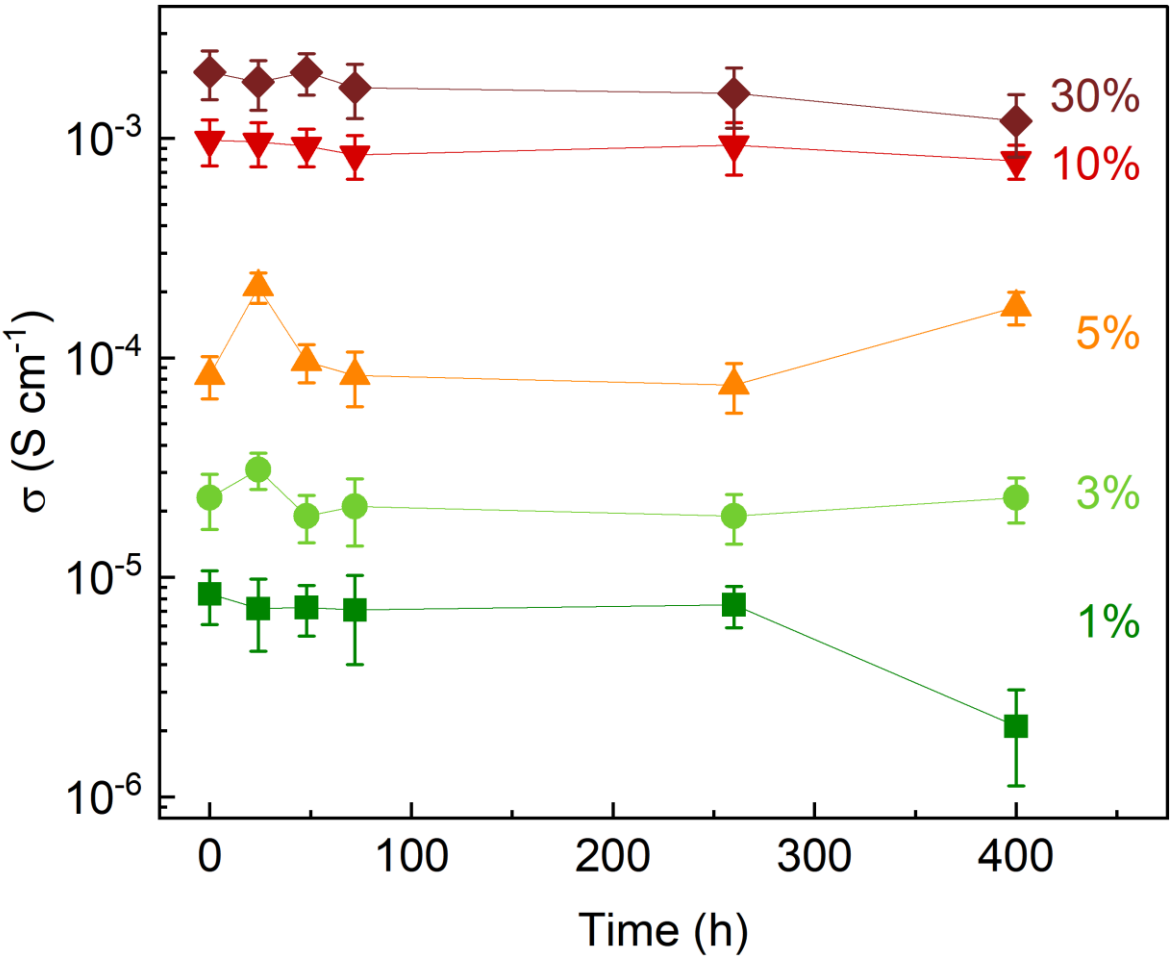

Figure 2. Electrical conductivity as a function of the aging time for DMBI-H/P(NDI2OD-T2) blends of different composition (from 1 wt% to 30 wt%).

According to the data shown in Figure 1, after 250 h of aging in the glove box, DMBI-H should be decomposed at around 50% and yet no effect is apparent from the electrical data. Of course, the assumption that the new samples behave identically to the NMR one, irrespectively of the presence of the polymer might be totally off target. We thus prepared a sample intentionally and majorly contaminated with DMBI-Ox. We doped P(NDI2OD-T2) at 10 wt% level with a 4:1 molar ratio mixture of DMBI-Ox and DMBI-H, corresponding to an active DMBI-H concentration of 2 wt%.

According to Figure 2 data, the corresponding conductivity value is expected to be within the $0.9 \cdot 10^{-5}$ S/cm recorded for the 1 wt% doped sample and the $2 \cdot 10^{-5}$ S/cm obtained for the 3 wt% sample. Instead, we obtained $0.9 \cdot 10^{-3}$ S/cm, a value almost two orders of magnitude higher than expected, and consistent with the conductivity observed for the 10% DMBI-H/P(NDI2OD-T2) blend prepared after 400 hours (which should be around 80% decomposed).

DMBI-Ox is not expected to contribute to the doping process. Nonetheless, we performed a control experiment using a 30 wt% blend of DMBI-Ox/P(NDI2OD-T2). After the standard thermal treatment, we obtained a conductivity of $6 \cdot 10^{-6}$ S/cm, a value which is an order of magnitude higher than the $0.3 \cdot 10^{-6}$ S/cm given by pure P(NDI2OD-T2). The very limited increase we observed, compared to doping with DMBI-H, could be explained by differences in the crystallinity of pure polymer and the blend.

DMBI-H is known to be poorly miscible with P(NDI2OD-T2), indeed the improvement of the mutual compatibility between *n*-type semiconductors and DMBI-like molecules represents a recognizable trend in the dedicated literature.[17,21,33] There is also a general consensus that only a fraction of the dopant molecules can efficiently reduce the polymers and contribute to the increase in the conductivity. This is a direct consequence of the phase segregation of the dopant, effectively reducing the interphase area between dopant and polymer.[34]

Our findings can be reconciliated with such an interpretation, once realized that DBMI-Ox is far less soluble than DMBI-H. The former could act as crystallization seed, thus favouring the formation of domains having different characteristics with respect to pure DMBI-H.

Differential scanning calorimetry (DSC) can give insight on the nature of the DMBI-H/DMBI-Ox interaction and help shedding light on our surprising results. Panels A and B in Figure 3 show the thermograms we obtained repeatedly melting and solidifying an analytically pure sample of DMBI-H. We carried out the experiments under N_2 flux and at a heating rate of 10 °C/min. The cooling curves are omitted as no transition was evident in all the cases. The first scan, carried out between 25 and 150 °C, shows only the sharp peak associated with the melting of DMBI-H at 108 °C. The second scan shows an exothermic peak at 74 °C, associated with cold crystallization of the sample, followed again by fusion at a slightly higher temperature of 109 °C. In the third heating cycle, the cold crystallization peak shifts at 60 °C and a new sharp endothermic peak appears at 98 °C, followed by the fusion of DMBI-H at 109 °C. In the fourth run, the exothermic crystallization peak is unchanged, but the only endothermic peak still visible is the one at 99 °C, whilst the original one at 109 °C is no longer visible. Suspecting a role played by thermally induced formation of DMBI-Ox, we prepared a sample having a DMBI-H/DMBI-Ox 99:1 molar composition and we compared the obtained DSC results. As observable in Figure 3C, in the first scan, the thermogram is identical to that of pure DMBI-H, as expected given that pure DMBI-Ox melts at 170 °C (see ESI). In the second scan (Figure 3D), the thermogram of the blend features

the cold crystallization exothermic peak - in this case at 52 °C - and both the endothermic peaks at 99 and 109 °C. The behaviour is very similar to that observed in the third scan of pure DMBI-H.

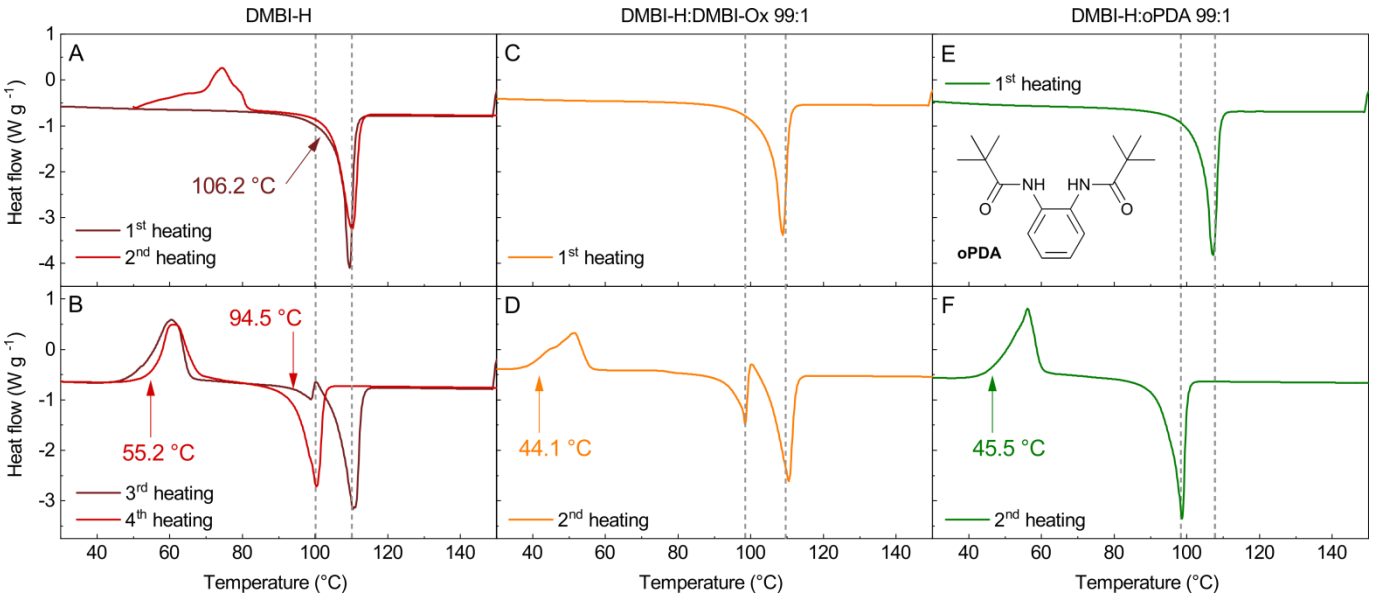

Figure 3. DSC plots for successive heating cycles of a DMBI-H sample (panel A and B), a DMBI-H:DMBI-Ox 99:1 sample (panel C and D), and a DMBI-H:oPDI 99:1 sample (panel E and F). Inset of panel E shows the structure of oPDA nucleating agent. Measurements carried out at 10 °C/min heating rate and under N_2 flux. Arrows point at the onset of the respective phase transition. Gray, dashed lines are guides to the eye.

The transition observed at 99 °C is related to the formation of a new phase that could be related to two distinct phenomena: a) the formation of a eutectic mixture between DMBI-Ox and DMBI-H or b) the seeded crystallization of a different polymorph of pure DMBI-H. Based on the thermal characterization alone a clear-cut assignment is not possible. The closer inspection of the shape of the 99 °C peak favours the polymorphism interpretation over the eutectic, essentially because in the latter case the melting peaks are generally broader. Irrespectively of the details about the nature of the new phase, its formation appears to be seeded by DMBI-Ox. To prove our point, we replaced DMBI-Ox with o-phenylenediamminebispivaloylammide (oPDA), a molecule acting as nucleating agent, and we repeated the DSC characterization, while keeping

constant the ratio between DMBI-H and impurity. As it is shown in Figure 3F, the oPDA/DMBI-H blend has a thermogram essentially identical to that we obtained for the fourth scan of pure DMBI-H. We observed the exothermic seeded crystallization at 50 °C (slightly lower than the 52 °C recorded in the case of the DMBI-Ox containing sample) and the sharp endothermic melting at 98 °C. The melting temperature of the new phase, as obtained in the presence of DMBI-Ox vs oPDA, is essentially identical.

The observed shift towards lower temperatures of the onset of the cold crystallization exotherm (from 55 °C of pure DMBI-H to 44-45 °C of the blend) also supports the hypothesis of an increasingly efficient heterogeneous nucleation as such characteristic (more commonly observed on the cooling scan) is a literature accepted way to compare efficiency of different nucleating agents.[35,36]

The remarkable analogy in the behaviour of oPDA and DMBI-Ox as contaminants in DMBI-H is also mirrored in the results of the electrical characterization. Table 1 summarizes the results we obtained while measuring the electrical conductivity of a series of oPDA:DMBI-H/ P(NDI2OD-T2) blends we prepared, thermally annealed and characterized under conditions identical to those employed for DMBI-H stability campaign.

Table 1. Electrical properties of oPDA:DMBI-H/ P(NDI2OD-T2) blends as a function of the respective composition.

Entry	oPDA:DMBI-H mol:mol	Doping level (wt%)	Conductivity (S/cm)	Enhancement[a]
1	Pure oPDA	30	$1.5 \cdot 10^{-6}$	-
2	80:20	10	$1.1 \cdot 10^{-3}$	-
3	1:99	3	$8.3 \cdot 10^{-5}$	4
4	1:99	5	$3.9 \cdot 10^{-4}$	5
5	1:99	10	$3.1 \cdot 10^{-3}$	3
6	1:99	30	$5 \cdot 10^{-3}$	2
7[b]	1:99	5	$9.2 \cdot 10^{-5}$	-
8[b]	1:99	10	$9.5 \cdot 10^{-4}$	-
9[b]	1:99	30	$1.8 \cdot 10^{-3}$	-

[a] With respect to a DMBI-H/P(NDI2OD-T2) blend having the same wt% concentration of pure DMBI-H; [b] annealed at 90°C instead of 150°C.

Firstly, we tested (entry 1) a 30 wt% oPDA blend in the polymer obtaining a conductivity of $1.5 \cdot 10^{-6}$ S/cm. This value is like that obtained for the 30 wt% DMBI-Ox blend and is likely connected to the same effect. We then tested (entry 2) a 10 wt% concentration of a 80:20 molar mixture of oPDA:DMBI-H, obtaining a conductivity of $1.1 \cdot 10^{-3}$ S/cm. The value is again in staggering agreement with the one we obtained using DMBI-Ox under the very same experimental conditions ($0.9 \cdot 10^{-3}$ S/cm).

According to the DSC data, a 1 mol% amount of oPDA over DMBI-H is enough to achieve efficient nucleation of the new phase. We consequently used a 99:1 mixture in the doping of P(NDI2OD-T2) and we compared the results obtained at the very same DMBI-H concentration, but in the absence of oPDA. In all of the cases, we obtained a clear boosting effect, particularly evident for the 3 wt% (entry 3) and the 5 wt% (entry 4) samples achieving a four and a fivefold enhancement. The 30 wt% sample gave a conductivity of $5 \cdot 10^{-3}$ S/cm, amongst the highest ever reported under similar experimental conditions for the DMBI-H/P(NDI2OD-T2) system. As a

further confirmation of the role played by heterogeneous nucleation, we repeated the 5, 10 and 30 wt% tests reducing the annealing temperature at 90 ° C. Under such conditions, the nucleation of the new phase is not possible as this would require melting of DMBI-H at 110 °C. Consistently, the conductivity values we observed are essentially identical to those obtained with pure DMBI-H.

Summing up the results of our electrical/thermal combined characterization, we can conclude that the reason why the formation of DMBI-Ox during handling of DMBI-H samples has been long overlooked is that its presence at small concentration does not negatively affect the electrical conductivity of the blend. On the contrary, once realized the very peculiar role played by DMBI-Ox in the complex ternary blend, it is even possible to exploit its presence to enhance performances. Although such effects had been previously observed and exploited in the optimization of conjugated polymers-fullerene blends for BHJ solar cells, to the best of our knowledge, they were not yet reported within in the context of molecular doping.[35–37]

Conclusions

We have demonstrated that DMBI-H, by far the most popular molecular dopant for n-type semiconducting materials, is not as stable as the dedicated literature might suggest. We have also shown that the main decomposition product formed during aging in the processing solvent is the Amide DMBI-Ox rather than the cation $DMBI^+$. The former plays a crucial role in determining the microstructure of DMBI-H/n-type polymer blends, dramatically enhancing performances.

We believe that our findings significantly change the design guidelines for new doping strategies involving DMBI-H like compounds and n-type polymers. Rather than focusing exclusively on increasing the mutual miscibility of the two components, a characteristic helping doping efficiency but negatively affecting charge carriers mobility, attention should be focused on the solid-state microstructure of such blends and the nature of the phases and interphases involved. Indeed, our data show that the very same dopant can be present in two different phase segregated forms, one melting at 108-110 °C and the other at 98-99 °C. The very same data also suggests that nucleation of the latter is strongly enhanced in the presence of nucleating agents in the form of decomposition products (DMBI-Ox) or exogenous additive (oPDA). Such seeded nucleation appears to have a striking effect on the doping process.

Although no conclusion can be currently drawn on this respect, it has not escaped our notice that such observation hints at an interfacial doping mechanism between two different phases rather than on a more simplistic dissolution of the dopant into the polymer phase. In such a scenario, roughly reminiscent of the case of fullerene-polymer blends, heterogeneous nucleation is expected to play a key role on the extension of phase segregation, microstructure, polymorphism, and reactivity during doping. Moreover, as the final doped blend behaves as a heterogenous mixed ionic conductor, the same factors likely play a role on the overall electronic and ionic conductivities deeply affecting performances of final devices.[38]

We believe that our findings will prompt a rigorous screening of different nucleating agents, aiming at achieving both higher electrical performance and a deeper understanding of the underlying phenomena in complex blends of polymers and molecular dopants.

Notes and references

1 I. Salzmann and G. Heimel, *Journal of Electron Spectroscopy and Related Phenomena*, 2015, **204**, 208–222.

2 Y. Zhang, H. Zhou, J. Seifter, L. Ying, A. Mikhailovsky, A. J. Heeger, G. C. Bazan and T.-Q. Nguyen, *Advanced Materials*, 2013, **25**, 7038–7044.

3 I. E. Jacobs and A. J. Moulé, *Advanced Materials*, 2017, **29**, 1703063.

4 Y. Lin, Y. Firdaus, M. I. Nugraha, F. Liu, S. Karuthedath, A. Emwas, W. Zhang, A. Seitkhan, M. Neophytou, H. Faber, E. Yengel, I. McCulloch, L. Tsetseris, F. Laquai and T. D. Anthopoulos, *Adv. Sci.*, 2020, **7**, 1903419.

5 S. Reineke, F. Lindner, G. Schwartz, N. Seidler, K. Walzer, B. Lüssem and K. Leo, *Nature*, 2009, **459**, 234–238.

6 U. Ail, M. J. Jafari, H. Wang, T. Ederth, M. Berggren and X. Crispin, *Adv. Funct. Mater.*, 2016, **26**, 6288–6296.

7 Q. Jiang, H. Sun, D. Zhao, F. Zhang, D. Hu, F. Jiao, L. Qin, V. Linseis, S. Fabiano, X. Crispin, Y. Ma and Y. Cao, *Adv. Mater.*, 2020, **32**, 2002752.

8 J. Liu, G. Ye, B. van der Zee, J. Dong, X. Qiu, Y. Liu, G. Portale, R. C. Chiechi and L. J. A. Koster, *Adv. Mater.*, 2018, **30**, 1804290.

9 J. Liu, Y. Shi, J. Dong, M. I. Nugraha, X. Qiu, M. Su, R. C. Chiechi, D. Baran, G. Portale, X. Guo and L. J. A. Koster, *ACS Energy Lett.*, 2019, **4**, 1556–1564.

10 M. Xiong, X. Yan, J.-T. Li, S. Zhang, Z. Cao, N. Prine, Y. Lu, J.-Y. Wang, X. Gu and T. Lei, *Angewandte Chemie International Edition*, 2021, **60**, 8189–8197.

11 D. Kiefer, R. Kroon, A. I. Hofmann, H. Sun, X. Liu, A. Giovannitti, D. Stegerer, A. Cano, J. Hynynen, L. Yu, Y. Zhang, D. Nai, T. F. Harrelson, M. Sommer, A. J. Moulé, M. Kemerink, S. R. Marder, I. McCulloch, M. Fahlman, S. Fabiano and C. Müller, *Nature Mater*, 2019, **18**, 149–155.

12 I. Salzmann, G. Heimel, M. Oehzelt, S. Winkler and N. Koch, *Acc. Chem. Res.*, 2016, **49**, 370–378.

13 Y. Yamashita, J. Tsurumi, M. Ohno, R. Fujimoto, S. Kumagai, T. Kurosawa, T. Okamoto, J. Takeya and S. Watanabe, *Nature*, 2019, **572**, 634–638.

14 P. Pingel and D. Neher, *Phys. Rev. B*, 2013, **87**, 115209.

15 J. Li, G. Zhang, D. M. Holm, I. E. Jacobs, B. Yin, P. Stroeve, M. Mascal and A. J. Moulé, *Chem. Mater.*, 2015, **27**, 5765–5774.

16 J. E. Anthony, A. Facchetti, M. Heeney, S. R. Marder and X. Zhan, *Advanced Materials*, 2010, **22**, 3876–3892.

17 J. Liu, L. Qiu, R. Alessandri, X. Qiu, G. Portale, J. Dong, W. Talsma, G. Ye, A. A. Sengrian, P. C. T. Souza, M. A. Loi, R. C. Chiechi, S. J. Marrink, J. C. Hummelen and L. J. A. Koster, *Adv. Mater.*, 2018, **30**, 1704630.

18 A. Werner, F. Li, K. Harada, M. Pfeiffer, T. Fritz, K. Leo and S. Machill, *Advanced Functional Materials*, 2004, **14**, 255–260.

19 V. A. Kolesov, C. Fuentes-Hernandez, W.-F. Chou, N. Aizawa, F. A. Larrain, M. Wang, A. Perrotta, S. Choi, S. Graham, G. C. Bazan, T.-Q. Nguyen, S. R. Marder and B. Kippelen, *Nature Mater*, 2017, **16**, 474–480.

20 Y. Zeng, W. Zheng, Y. Guo, G. Han and Y. Yi, *J. Mater. Chem. A*, 2020, **8**, 8323–8328.

21 B. Saglio, M. Mura, M. Massetti, F. Scuratti, D. Beretta, X. Jiao, C. R. McNeill, M. Sommer, A. Famulari, G. Lanzani, M. Caironi and C. Bertarelli, *J. Mater. Chem. A*, 2018, **6**, 15294–15302.

22 B. D. Naab, S. Zhang, K. Vandewal, A. Salleo, S. Barlow, S. R. Marder and Z. Bao, *Advanced Materials*, 2014, **26**, 4268–4272.

23 B. D. Naab, S. Guo, S. Olthof, E. G. B. Evans, P. Wei, G. L. Millhauser, A. Kahn, S. Barlow, S. R. Marder and Z. Bao, *Journal of the American Chemical Society*, 2013, **135**, 15018–15025.

24 X.-Q. Zhu, M.-T. Zhang, A. Yu, C.-H. Wang and J.-P. Cheng, *J. Am. Chem. Soc.*, 2008, **130**, 2501–2516.

25 S. Jhulki, H.-I. Un, Y.-F. Ding, C. Risko, S. K. Mohapatra, J. Pei, S. Barlow and S. R. Marder, *Chem*, 2021, **7**, 1050–1065.

26 E. Hasegawa, N. Yoshioka, T. Tanaka, T. Nakaminato, K. Oomori, T. Ikoma, H. Iwamoto and K. Wakamatsu, *ACS Omega*, 2020, **5**, 7651–7665.

27 S. Riera-Galindo, A. Orbelli Biroli, A. Forni, Y. Puttisong, F. Tessore, M. Pizzotti, E. Pavlopoulou, E. Solano, S. Wang, G. Wang, T.-P. Ruoko, W. M. Chen, M. Kemerink, M. Berggren, G. di Carlo and S. Fabiano, *ACS Appl. Mater. Interfaces*, 2019, **11**, 37981–37990.

28 X.-Q. Zhu, M.-T. Zhang, A. Yu, C.-H. Wang and J.-P. Cheng, *J. Am. Chem. Soc.*, 2008, **130**, 2501–2516.

29 M. Xiong, X. Yan, J. Li, S. Zhang, Z. Cao, N. Prine, Y. Lu, J. Wang, X. Gu and T. Lei, *Angew. Chem.*, 2021, **133**, 8270–8278.

30 R. A. Schlitz, F. G. Brunetti, A. M. Glaudell, P. L. Miller, M. A. Brady, C. J. Takacs, C. J. Hawker and M. L. Chabinyc, *Adv. Mater.*, 2014, 6.

31 J. Liu, L. Qiu, R. Alessandri, X. Qiu, G. Portale, J. Dong, W. Talsma, G. Ye, A. A. Sengrian, P. C. T. Souza, M. A. Loi, R. C. Chiechi, S. J. Marrink, J. C. Hummelen and L. J. A. Koster, *Adv. Mater.*, 2018, **30**, 1704630.

32 Y. M. Gross, D. Trefz, C. Dingler, D. Bauer, V. Vijayakumar, V. Untilova, L. Biniek, M. Brinkmann and S. Ludwigs, *Chem. Mater.*, 2019, 14.

33 D. Kiefer, A. Giovannitti, H. Sun, T. Biskup, A. Hofmann, M. Koopmans, C. Cendra, S. Weber, L. J. Anton Koster, E. Olsson, J. Rivnay, S. Fabiano, I. McCulloch and C. Müller, *ACS Energy Lett.*, 2018, **3**, 278–285.

34 R. A. Schlitz, F. G. Brunetti, A. M. Glaudell, P. L. Miller, M. A. Brady, C. J. Takacs, C. J. Hawker and M. L. Chabinyc, *Advanced Materials*, 2014, **26**, 2825–2830.

35 N. D. Treat, J. A. Nekuda Malik, O. Reid, L. Yu, C. G. Shuttle, G. Rumbles, C. J. Hawker, M. L. Chabinyc, P. Smith and N. Stingelin, *Nature Materials*, 2013, **12**, 628–633.

36 C. Lindqvist, J. Bergqvist, C.-C. Feng, S. Gustafsson, O. Bäcke, N. D. Treat, C. Bounioux, P. Henriksson, R. Kroon, E. Wang, A. Sanz-Velasco, P. M. Kristiansen, N. Stingelin, E. Olsson, O. Inganäs, M. R. Andersson and C. Müller, *Advanced Energy Materials*, 2014, **4**, 1301437.

37 H. Lu, Y. Wu, W. Li, H. Wei, W. Ma and Z. Bo, *ACS Appl. Mater. Interfaces*, 2015, **7**, 18924–18929.

38 B. D. Paulsen, K. Tybrandt, E. Stavrinidou and J. Rivnay, *Nature Materials*, 2020, **19**, 13–26.